Supplementary Information (SI) for Chemical Science.
This journal is © The Royal Society of Chemistry 2024

Enhancing the Performance of Molecule-Based Piezoelectric Sensors by Optimizing Their Microstructures

Zheng-Xiao Tang, Bin Wang, Zhi-Rui Li, Zhuo Huang, Hai-Xia Zhao,* La-Sheng Long,* Lan-Sun Zheng

State Key Laboratory of Physical Chemistry of Solid Surfaces and Department of Chemistry, College of Chemistry and Chemical Engineering, Xiamen University, Xiamen, 361005, Fujian. China.

MEASUREMENT DETAILS:

All chemicals used in the synthesis were of reagent grade and were used without further purification.

X-ray crystallographic and powder X-ray diffraction (PXRD) measurements.

An Agilent Supernova CCD diffractometer utilizing Cu Kα radiation (λ = 1.54178 Å) in ω-scan mode ($\Delta\omega$ = 1.0°) was used for the collection of the single crystal data for **1** at 300 K. The CrysAlis PRO program was applied to execute data collection, cell refinement and data reduction. The structures were determined by direct methods using ShelXT and refined by full-matrix least squares on F^2 by using ShelXL in the OLEX2 program. CCDC 2208701 (**1**) can be obtained free of charge from the Cambridge Crystallographic Data Centre and contain the supplementary crystallographic data for this paper. A Rigaku Ultima IV X-ray diffractometer was used for room temperature PXRD measurements.

Thermogravimetric analysis (TGA) and differential thermal analysis (DTA)

Thermogravimetric analysis and differential thermal analysis curve were collected on a STA-449-F5 Jupiter from Netzsch at the rate of 10 K min^{-1} under the air atmosphere.

SHG measurements

Optical second harmonic generation (SHG) measurements were carried out with an integrated instrument, which ensured low divergence (pulsed Nd:YAG at a wavelength of 1064 nm, 10 Hz repetition rate, 1.6 MW peak power, 5 ns pulse duration) for the unexpanded laser (OPOTEK, 355 II). SHG experiments were performed using powder of **1** at room temperature.

d_{33} measurement

The polycrystalline films fabricated by powder of **1** were firstly poled on a high-voltage polarization device (DW-P303-1ACDF0, DONG WEN VOLTAGE, China) before d_{33} testing. The d_{33} was measured on a ZJ-6A (Institute of Acoustics, China).

Polarization−electric field (*P-E*) hysteresis loop measurements.

Polarization−electric field (*P-E*) hysteresis loop was measured using a Radiant Precision Premier II analyzer. To eliminate small electric conductivity contributions, the positive up negative down (PUND) method was employed. The polycrystalline thin films were fabricated by slowly evaporating a drop of saturated aqueous solution of **1** onto cleaned ITO-coated glass. The *P-E* hysteresis loop measurements were conducted using a capacitor structure composed of a copper column electrode, polycrystalline thin film and ITO-coated glass, with the copper column electrode serving as the top electrode and conductive ITO as the bottom electrode, respectively.

SEM measurements.

All types of composite films were observed using a ZEISS Sigma scanning electron microscope from ZEISS and SU8600 from Hitachi.

Open-circuit voltage and short-circuit current measurements.

The piezoelectric open-circuit voltage and short-circuit current of composite film devices with **1** were recorded with a Keithley electrometer (6517B).

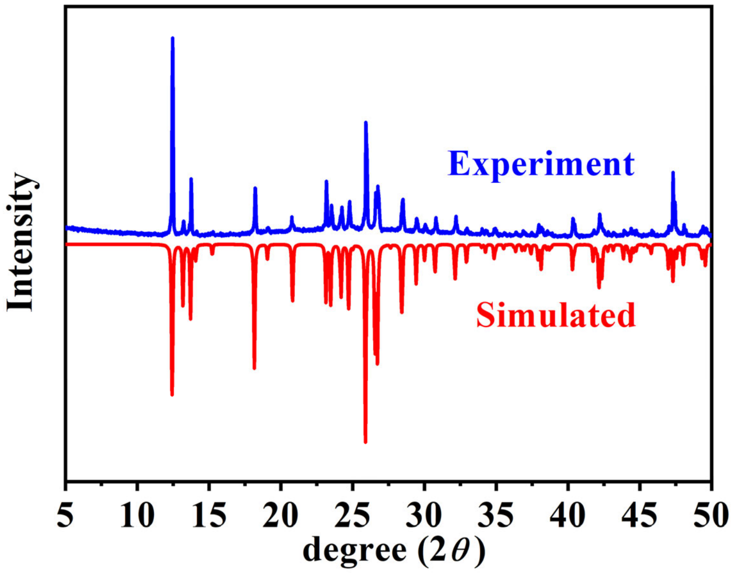

Figure S1 PXRD patterns of **1** at room temperature.

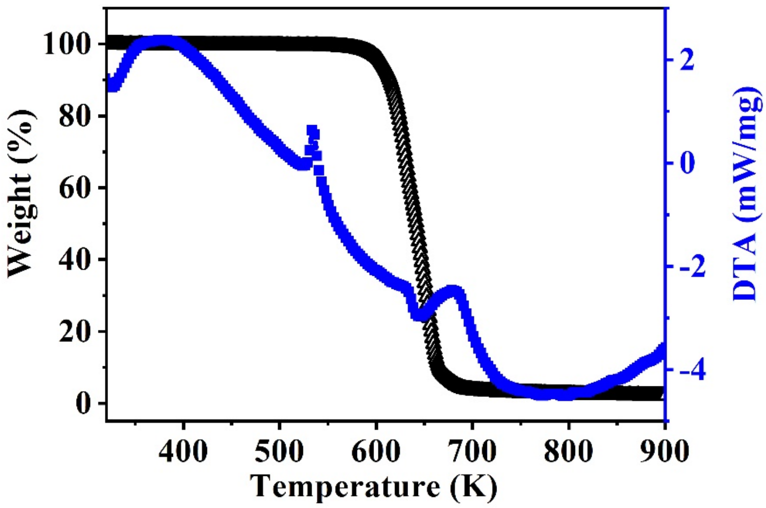

Figure S2 TG and DTA curve of **1.**

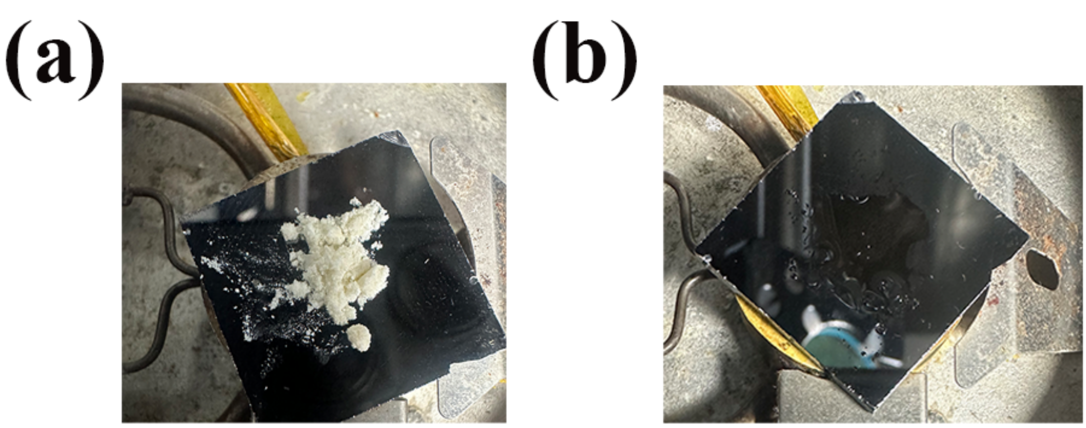

Figure S3 Optical images of **1**: (a) powder of **1**, (b) melt of **1**.

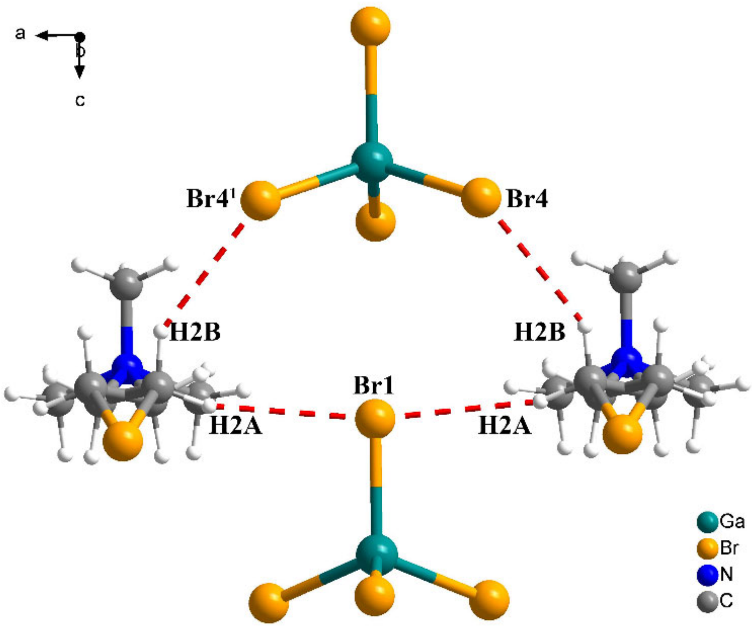

Figure S4 The Br···H—C distance between adjacent $[GaBr_4]^-$ anions and $[(CH_3)_3NCH_2CH_2Br]^+$ cations (Br1···H2A—C2: 3.779 Å; Br4···H2B—C2: 3.668 Å, ^{1}-X,+Y,+Z).

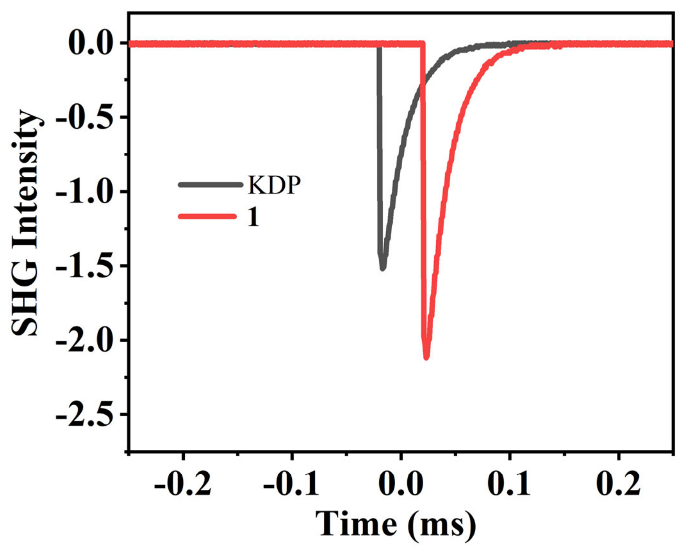

Figure S5 SHG signal of **1** at room temperature.

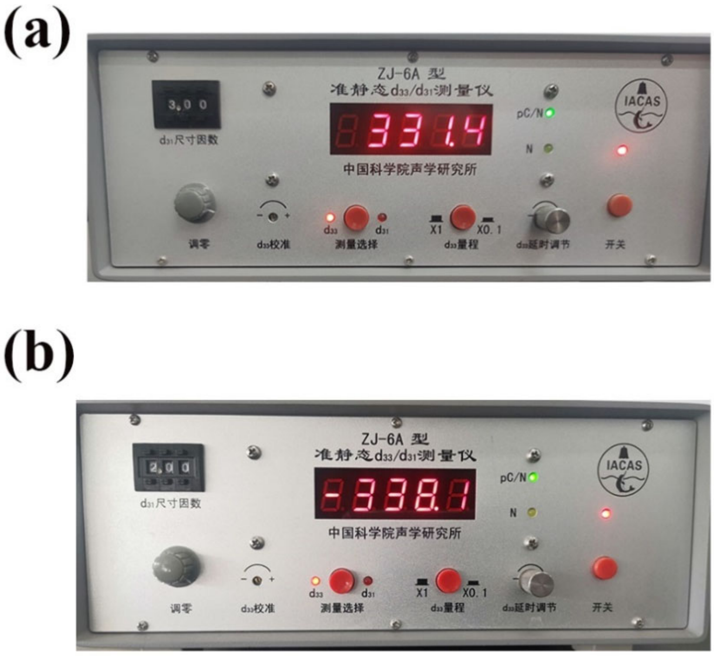

Figure S6 Piezoelectric d_{33} data of **1** (polycrystalline films): (a) forward in up connection, (b) reverse in down connection.

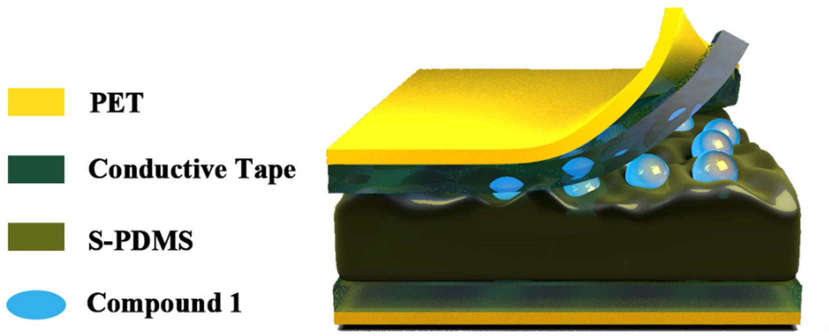

Figure S7 Schematic of the **1**@S-PDMS sensor device structure.

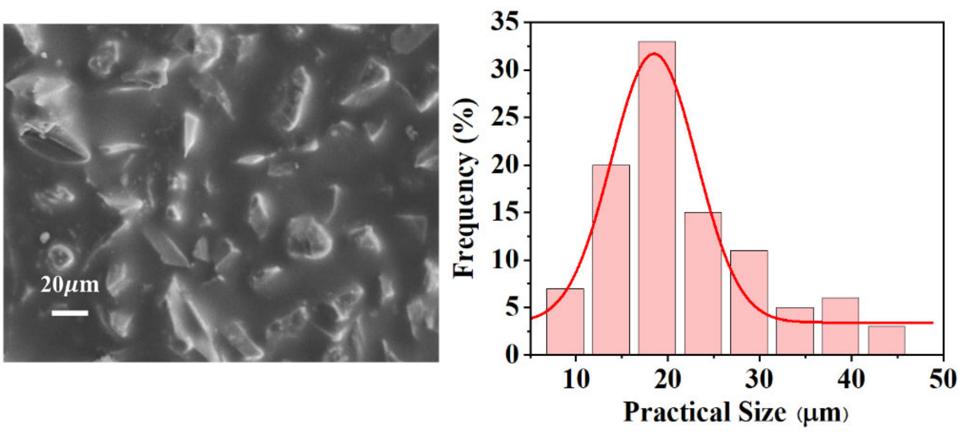

Figure S8 SEM image of sandpaper (P800) and pore size distributions.

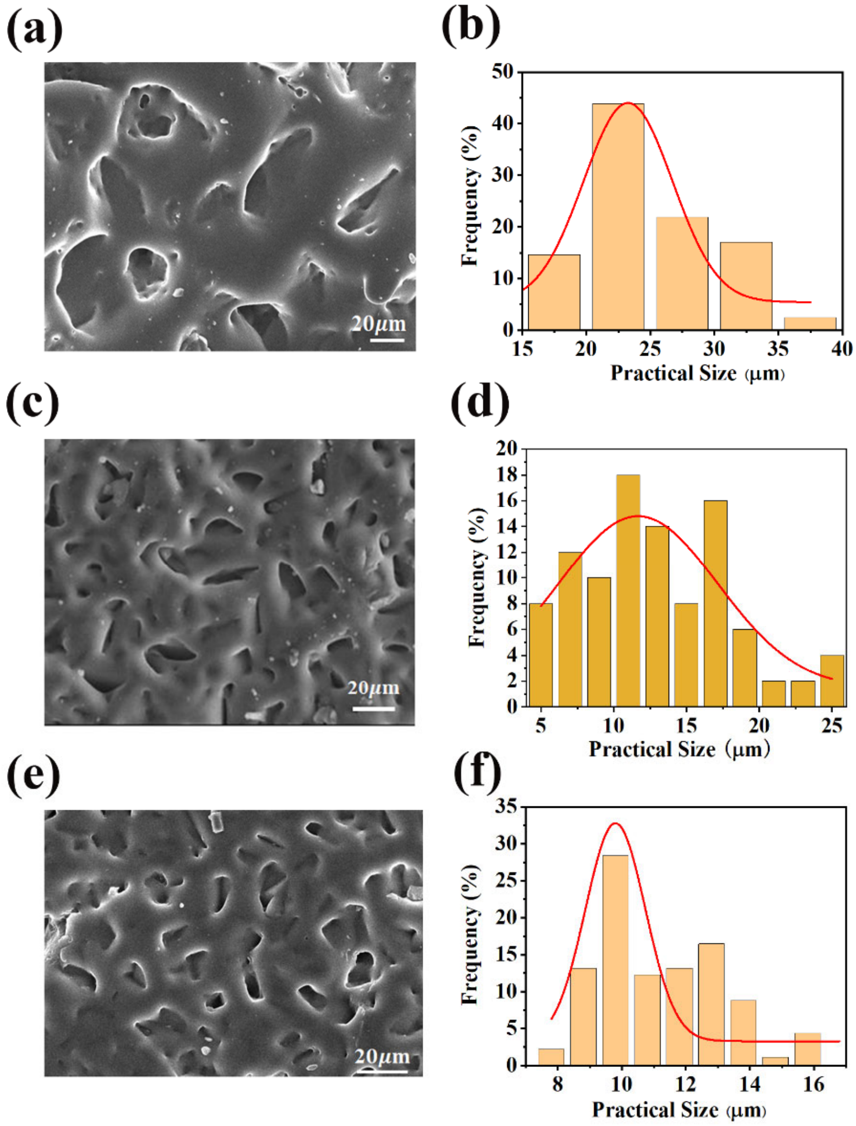

Figure S9 SEM images of S-PDMS: (a) 600#, (c) 1200#, (e) 1500# and pore size distributions: (b) 600#, (d) 1200#, (f) 1500#.

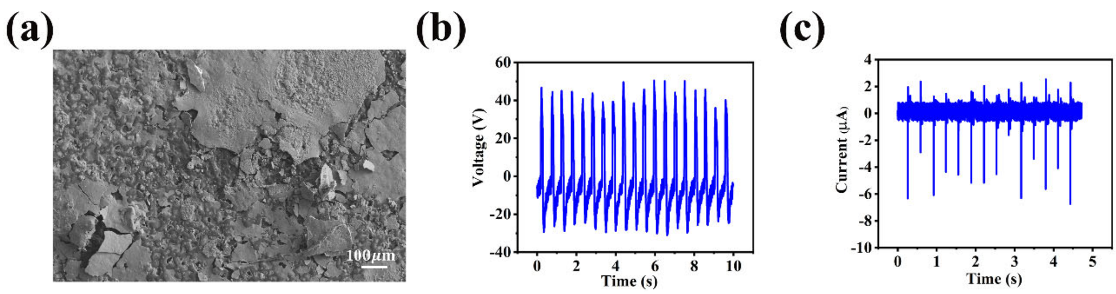

Figure S10 (a) SEM image of **1**@S-PDMS(800#) (spin-coating at 7 cycles without isopropanol); V_{oc} (b) and I_{sc} (c) for **1**@S-PDMS(800#) (spin-coating at 7 cycles without isopropanol).

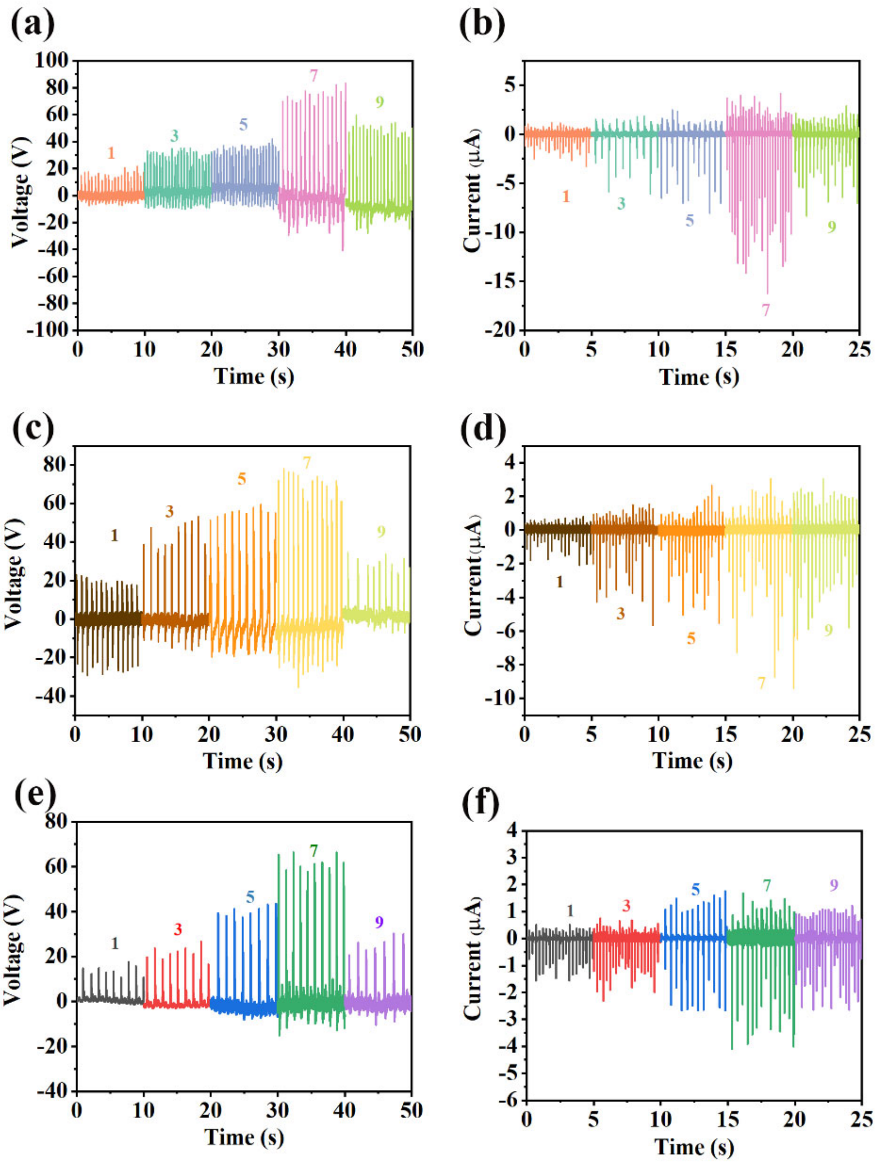

Figure S11 V_{oc}: (a) 600#, (c) 1200#, (e) 1500# and I_{sc}: (b) 600#, (d) 1200#, (f) 1500# of **1**@S-PDMS.

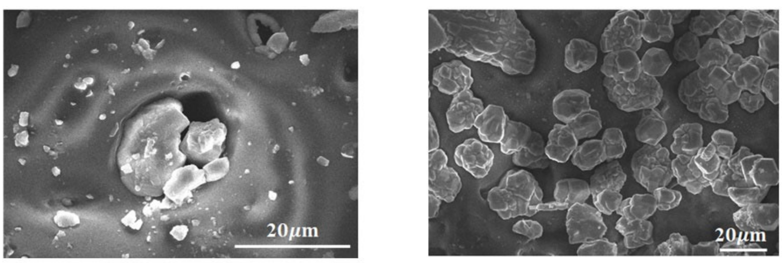

Figure S12 1 aggregate on S-PDMS(800#) when the spin-coating cycles exceed seven.

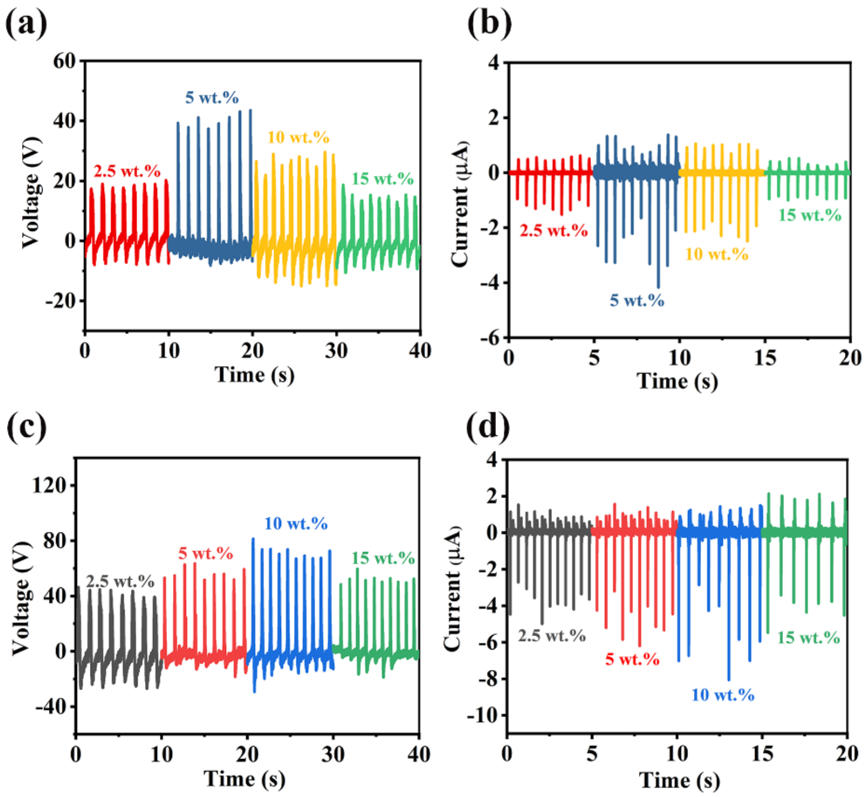

Figure S13 V_{oc}: (a) **1**-Flat-PDMS, (c) **1**-S-PDMS and I_{sc}: (b) **1**-Flat-PDMS, (d) **1**-S-PDMS with different mass fractions using 20 N palm pressure.

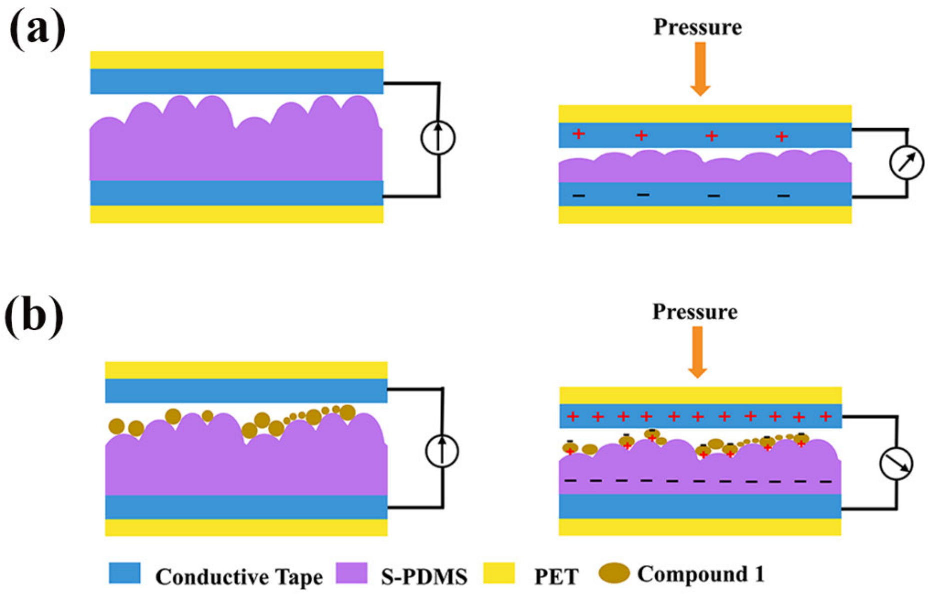

Figure S14 (a) Working mechanism of the triboelectric energy harvester. (b) Working mechanism of the hybrid energy harvester that integrated the piezoelectric and triboelectric energy harvester.

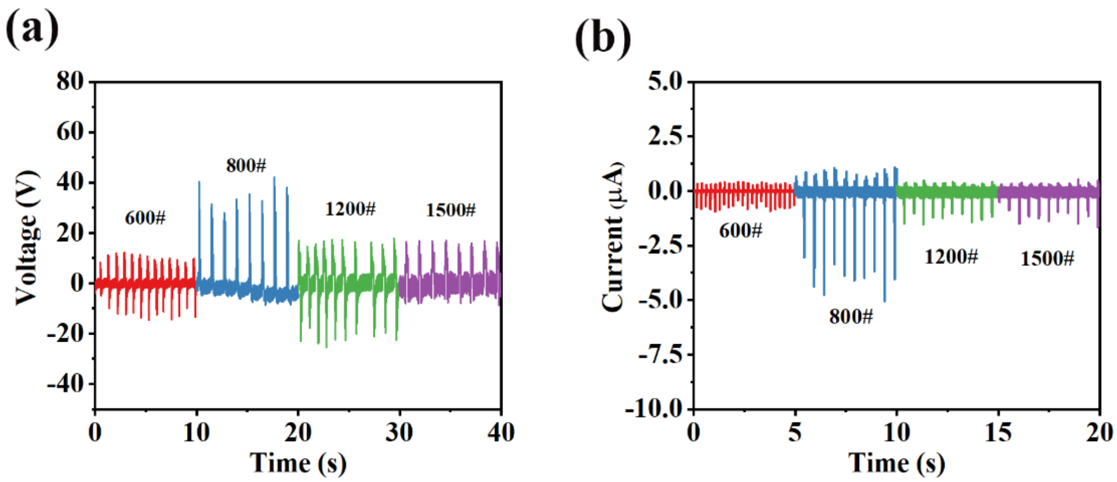

Figure S15 V_{oc} (a) and I_{sc} (b) for S-PDMS(600#, 800#, 1200#, 1500#).

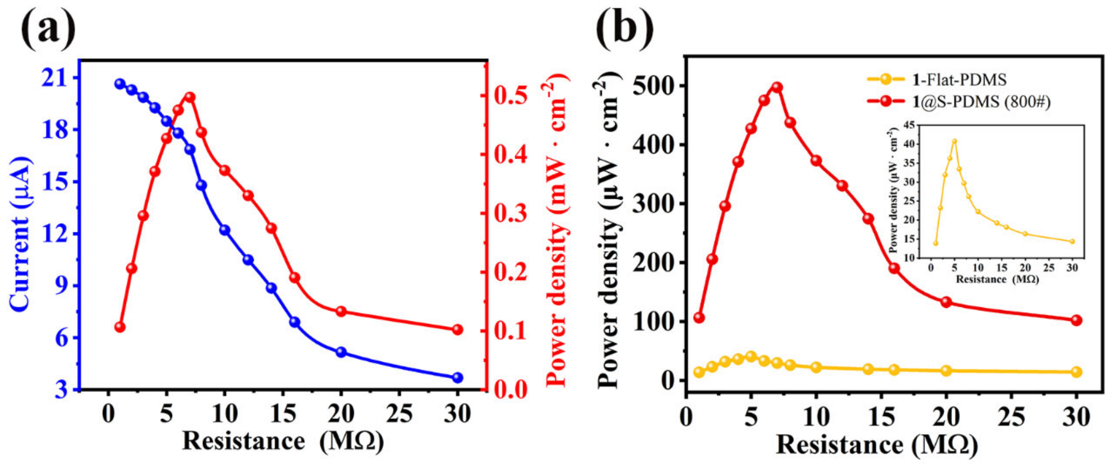

Figure S16 (a) The output current and power density under the condition of load resistances corresponding to the best performance device (**1**@S-PDMS(800#) (spin-coating at 7 cycles). (b) Power density of **1**-Flat-PDMS (mass fraction of powder **1** is 5%).

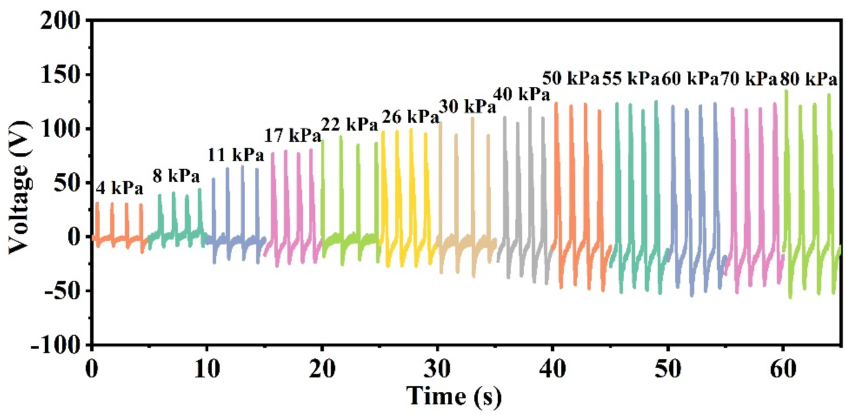

Figure S17 The voltage output of **1**@S-PDMS(800#) (spin-coating at 7 cycles) under various palm stresses.

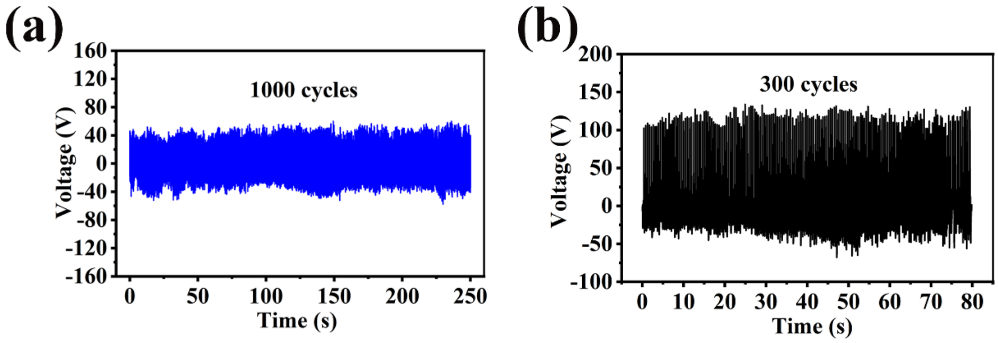

Figure S18 Voltage output stability of the **1**@S-PDMS(800#) (spin-coating at 7 cycles) sensor device under various palm stresses: (a) With 10 kPa palm stress. (b) With 70 kPa palm stress.

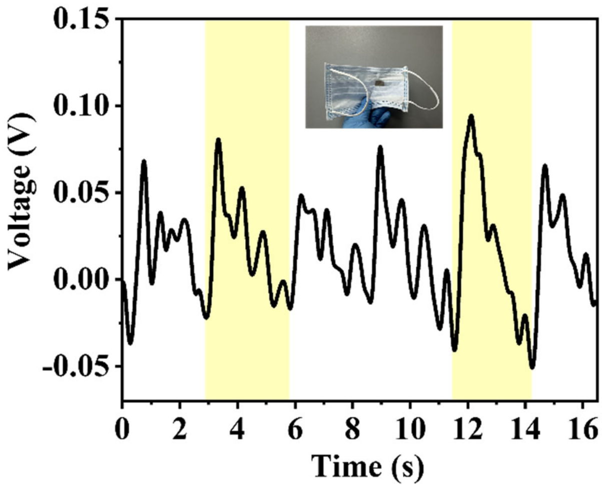

Figure S19 Signal responses corresponding to air pressure during breathing when the sensor was attached to the face mask.

Table S1 Crystal data and structure refinement of 1 at 300 K.

Compound	**1**
Empirical formula	$C_5H_{13}Br_5GaN$
Formula weight	556.43
Temperature (K)	300(1)
Crystal system	Orthorhombic
Space group	$Cmc2_1$
a (Å)	8.5264(3)
b (Å)	12.9009(3)
c (Å)	13.4160(4)
α (deg.)	90
β (deg.)	90
γ (deg.)	90
V (Å^3)	1475.74(8)
Z	4
ρ_{cal} (g · cm^{-3})	2.504
μ (mm^{-1})	13.003
F(000)	1024.0
Reflections collected	2419
R_{int}	0.0309
Data / restraints / parameters	1094/0/53
GOOFs	1.092
R_1/wR_2 $[I > 2\sigma(I)]$	R_1 = 0.0455, wR_2 = 0.1144
R_1/wR_2 (all data)	R_1 = 0.0491, wR_2 = 0.1167
Largest diff. peak/hole (e · Å^{-3})	0.86/-0.80

Table S2 Calculation of *Ps*.

Temperature (K)	Dipole moment (Debye)	Saturated polarization (μC cm^{-2})
300	54.9004	12.28

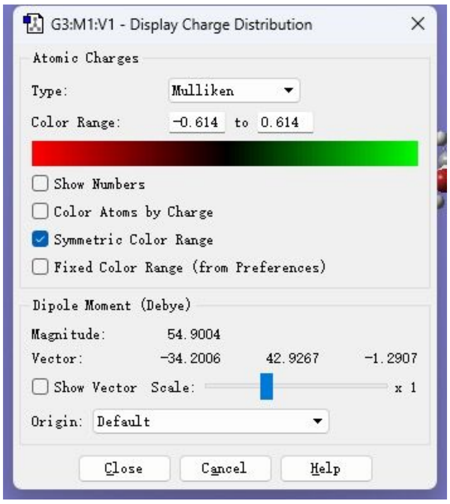

According to the crystal structure data collected at 300 K, the dipole moment of the crystal cell: μ = 26.3785 Debye, based on the G2:M1:V1-Display Charge Distribution calculations;

$P_s = \sum Ze\Delta r/V = 54.9004 \times 10^{-18}$ esu·cm / ($1475.74(8) \times 10^{-30}$ m^3) ≈ 0.122766 C m^2 = 12.28 μC cm^{-2}

Table S3 A summary of the output performance of the molecule-based ferroelectric composite films and energy harvesting devices of inorganic ceramics which combine the piezoelectric and triboelectric.

Piezoelectric Materials and substrate	Working Mechanism	V_{oc} (V)	J_{sc} (μA/cm^2)	Power density (μW/cm^2)	ref
$[(CH_3)_3NCH_2CH_2Cl][GaBr_4]$-PDMS	Piezoelectric	179	6.4 μA	120	1
MA-$SnBr_3$-PDMS	Piezoelectric	18.8	13.76	74.52	2
FA-$PbBr_3$-PDMS	Piezoelectric	8.5	3.8	12	3
MA-SnI_3-PVDF	Piezoelectric	12	4	21.6	4
FA-$PbBr_3$-PVDF	Piezoelectric	30	6.2	27.4	5
$[BnNMe_2{}^nPr]_2CdBr_4$-PDMS	Piezoelectric	63.8	0.59	37.1	6
HETMA-$CdCl_3$-PDMS	Piezoelectric	55.2	4.02	70.9	7
TMCM-$CdCl_3$-PDMS	Piezoelectric	41	3.45	115.2	8
$C_6H_5N(CH_3)_3CdBr_2Cl_{0.75}I_{0.25}$-PDMS	Piezoelectric	210	64	1100	9
PZT-Silicon rubber with PTFE particles	Piezoelectric Triboelectric	600	17 μA	111	10
PVDF and BTO nanofibre-PDMS	Piezoelectric Triboelectric	160	-	222	11
Ag NWS and BTO-PDMS	Piezoelectric Triboelectric	105	6.5	102	12
V-$NaNbO_3$-PDMS	Piezoelectric Triboelectric	200	5.7 μA	480	13
BTO nano particles-Porous PDMS	Piezoelectric Triboelectric	280	5.6 μA	41	14
PVDF and Silk fibre	Piezoelectric Triboelectric	500	12 μA	310	15
BTO nanorods-CS	Piezoelectric Triboelectric	247	36.7	1570	16
3D-printed BTO-PDMS	Piezoelectric Triboelectric	405	38 μA	2200	17
$ZnSnO_3$ nanocubes-PDMS	Piezoelectric Triboelectric	400	7	750	18
Ca doped BZT-PDMS	Piezoelectric Triboelectric	550	34 μA	2360	19
ZnO nanoflakes-PDMS	Piezoelectric Triboelectric	470	60	28200	20
PVDF/TMCM-$MnCl_3$ (ultrasound-driven)	Piezoelectric Triboelectric	29.2	900 μA	1020	21
$[(CH_3)_3NCH_2CH_2Br][GaBr_4]$@S-PDMS	Piezoelectric Triboelectric	125	25 μA	490	This Work

Table S4 Comparison of the sensitivity and monitoring range of the materials based composite films on different mechanisms (piezoelectric, triboelectric, synergy of piezoelectric and triboelectric).

Piezoelectric Materials	Working Mechanism	Sensitivity	Monitoring Range	ref
$[C(NH_2)_3]ClO_4$-PU	Piezoelectric	170 mV/kPa (0-1 kPa) 40 mV/kPa (1-5 kPa)	0-5 kPa	22
ZnO-PAN/MXene/PDA	Piezoelectric	28.56 V/N (0-2 N)	0-2 N	23
PVDF and GS-PVDF	Piezoelectric	0.83 V/N (0-6 N)	0-6 N	24
dabcoH-ReO_4-PVDF	Piezoelectric	0.38 V/N (1-10 N)	1-10 N	25
ZnS:Cu-PAN	Piezoelectric	2.46 V/N (0.1-1.96 N)	0.1-1.96 N	26
Nb_2CT_x-PDMS and BTO-PVDF	Piezoelectric	16.1 V/N (0.1-0.6 N) 0.39 V/N (0.6-30 N)	0.1-30 N	27
UiO-66-NO_2-PAN	Piezoelectric	5.62 V/N (1-20 N) 0.88 V/N (20-160 N)	1-160 N	28
PZT nano particles-P(VDF-TrFE)	Piezoelectric	1.38 V/kPa (0-32 kPa) 0.81 V/kPa (32-128 kPa)	0-128 kPa	29
GaN@PDMS	Piezoelectric	14.25 V/kPa (0-1.6 kPa)	0-1.6 kPa	30
Liquid metal based PDMS sponge	Triboelectric	0.44 V/N (20-101 N)	20-101 N	31
Micropatterend PDMS	Triboelectric	44.31 V/kPa (0-2 kPa) 7.16 V/kPa (2-8 kPa)	0-8kPa	32
ZnO/C-PVDF	Piezoelectric Triboelectric	2.44 V/N (0-16 N)	0-16 N	33
PVDF and PTFE and Nylon	Piezoelectric Triboelectric	1.3 V/N (0.4-1.6 N) 6.2 V/N (1.6-2.8 N)	0.4-2.8 N	34
3D-printed BTO-PDMS	Piezoelectric Triboelectric	2 V/N (0-60 N) 1.6 V/N (60-220 N)	0-220 N	17

BTO-PDMS	Piezoelectric Triboelectric	0.3 V/kPa (0-200 kPa) 0.05 V/kPa (200-800 kPa)	0-800 kPa	35
PZT−PEDOT:PSS	Piezoelectric Triboelectric	0.23 V/N (0-12N)	0-12 N	36
BTO nano particles-Porous PDMS	Piezoelectric Triboelectric	2.1 V/cm (a 6.2 g ball drop from different heights)	10-60 cm (Height)	14
PVDF/TMCM-$MnCl_3$ (mechanical force)	Piezoelectric Triboelectric	6.21 V/kPa	-	21
$[(CH_3)_3NCH_2CH_2Br][GaBr_4]$@S-PDMS	Piezoelectric Triboelectric	3.57 V/kPa (0-24 kPa) 1.02 V/kPa (24-45 kPa)	0-45 kPa	This work

Notes and references

1 B. Wang, Z. R. Li, Z. X. Tang, H. X. Zhao, L. S. Long, L. S. Zheng, *Chem. Sci.,* 2024, **15**, 15192.

2 S. Ippili, V. Jella, J. Kim, S. Hong, S. G. Yoon, *ACS Appl. Mater. Interfaces*, 2020, **12**, 16469.

3 R. Ding, H. Liu, X. Zhang, J. Xiao, R. Kishor, H. Sun, B. Zhu, G. Chen, F. Gao, X. Feng, J. Chen, X. Chen, X. Sun, Y. Zheng, *Adv. Funct. Mater.*, 2016, **26**, 7708.

4 S. Ippili, V. Jella, J. H. Eom, J. Kim, S. Hong, J. S. Choi, V. D. Tran, N. Van Hieu, Y. J. Kim, H. J. Kim, S. G. Yoon, *Nano Energy*, 2019, **57**, 911.

5 R. Ding, X. Zhang, G. Chen, H. Wang, R. Kishor, J. Xiao, F. Gao, K. Zeng, X. Chen, X. W. Sun, Y. Zheng, *Nano Energy*, 2017, **37**, 126.

6 S. Deswal, S. K. Singh, P. Rambabu, P. Kulkarni, G. Vaitheeswaran, B. Praveenkumar, S. Ogale, R. Boomishankar, *Chem. Mater.*, 2019, **31**, 4545.

7 S. Deswal, S. K. Singh, R. Pandey, P. Nasa, D. Kabra, B. Praveenkumar, S. Ogale, R. Boomishankar, *Chem. Mater.*, 2020, **32**, 8333.

8 Y. J. Gong, Z. G. Li, H. Chen, T. M. Guo, F.-F. Gao, G.-J. Chen, Y. Zhang, Y. M. You, W. Li, M. He, X. H. Bu, J. Yu, *Matter*, 2023, **6**, 2066.

9 Y. Hu, K. Parida, H. Zhang, X. Wang, Y. Li, X. Zhou, S. A. Morris, W. H. Liew, H. Wang, T. Li, F. Jiang, M. Yang, M. Alexe, Z. Du, C. L. Gan, K. Yao, B. Xu, P. S. Lee, H. J. Fan, *Nature Commun.*, 2022, **13**, 5607.

10 J. He, S. Qian, X. Niu, N. Zhang, J. Qian, X. Hou, J. Mu, W. Geng, X. Chou, *Nano Energy*, 2019, **64**, 103933.

11 J. Song, B. Yang, W. Zeng, Z. Peng, S. Lin, J. Li, X. Tao, *Adv. Mater. Technologies*, 2018, **3**, 1800016.

12 X. Chen, K. Parida, J. Wang, J. Xiong, M. F. Lin, J. Shao, P. S. Lee, *ACS Appl. Mater. Interfaces*, 2017, **9**, 42200.

13 M. V. Paranjape, J. Kim, Y. Kim, E. Jo, S. A. Graham, P. Manchi, J. K. Lee, J. S. Yu, *Composites Science and Technology*, 2023, **242**, 110195.

14 M. Sahu, V. Vivekananthan, S. Hajra, D. K. Khatua, S. J. Kim, *Applied Materials*

Today, 2021, **22**, 100900.

15 Y. Guo, X. S. Zhang, Y. Wang, W. Gong, Q. Zhang, H. Wang, J. Brugger, *Nano Energy*, 2018, **48**, 152.

16 S. Pongampai, T. Charoonsuk, N. Pinpru, P. Pulphol, W. Vittayakorn, P. Pakawanit, N. Vittayakorn, *Composites Part B: Engineering*, 2021, **208**, 108602.

17 K. K. Meena, I. Arief, A. K. Ghosh, H. Liebscher, S. Hait, J. Nagel, G. Heinrich, A. Fery, A. Das, *Nano Energy*, 2023, **115**, 108707.

18 G. Wang, Y. Xi, H. Xuan, R. Liu, X. Chen, L. Cheng, *Nano Energy*, 2015, **18**, 28.

19 H. Patnam, B. Dudem, N. R. Alluri, A. R. Mule, S. A. Graham, S. J. Kim, J. S. Yu, *Composites Science and Technology*, 2020, **188**, 107963.

20 W. He, Y. Qian, B. S. Lee, F. Zhang, A. Rasheed, J. E. Jung, D. J. Kang, *ACS Appl. Mater. Interfaces*, 2018, **10**, 44415.

21 P. Chen, C. Cheng, X. Yang, T. Sha, X. Zou, F. Zhang, W. Jiang, Y. Xu, X. Cao, Y. M. You, Z. Luo, *ACS Nano*, 2023, **17**, 25625.

22 W. Li, C. Li, G. Zhang, L. Li, K. Huang, X. Gong, C. Zhang, A. Zheng, Y. Tang, Z. Wang, Q. Tong, W. Dong, S. Jiang, S. Zhang, Q. Wang, *Adv. Mater.*, 2021, **33**, 2104107.

23 Y. Huang, S. Chen, Y. Li, Q. Lin, Y. Wu, Q. Shi, *Chemical Engineering Journal*, 2024, **488**, 150997.

24 L. Lu, N. Zhao, J. Liu, B. Yang, *J. Mater. Chem. C*, 2021, **9**, 9309.

25 Q. Li, W. Ke, T. Chang, Z. Hu, *J. Mater. Chem. C*, 2019, **7**, 1532.

26 Y. Huang, R. Xue, L. An, Q. Shi, W. Zhang, Y. Wu, R. Liu, *Smart Mater. Struct.*, 2023, **32**, 095018.

27 C. Cao, P. Zhou, J. Wang, M. Liu, P. Wang, Y. Qi, T. Zhang, *Journal of Colloid and Interface Science*, 2024, **664**, 902.

28 Q. Lin, S. Chen, Y. Huang, H. Wang, Y. Wu, Y. Jin, R. Liu, Q. Shi, Y. Liang, *Polymer*, 2024, **304**, 127162.

29 J. Wang, Y. Fu, F. Liu, C. Cao, M. Liu, L. Yu, P. Zhou, X. Shang, G. Wang, T. Zhang, Y. Qi, *Sensors and Actuators A: Physical*, 2024, **374**, 115473.

30 A. Waseem, M. A. Johar, M. A. Hassan, I. V. Bagal, A. Abdullah, J.-S. Ha, J. K. Lee, S. W. Ryu, *Journal of Alloys and Compounds*, 2021, **872**, 159661.

31 Y. Wang, C. Zhao, L. Chen, Q. Wu, Z. Zhao, J. J. Lv, S. Wang, S. Pan, M. Xu, Y. Chen, H. Jin, *Nano Energy*, 2024, **127**, 109808.

32 Y. Zhong, J. Wang, L. Han, S. Dai, H. Zhu, J. Hua, G. Cheng, J. Ding, *Sensors and Actuators A: Physical*, 2023, **349**, 114013.

33 X. Li, D. Ji, B. Yu, R. Ghosh, J. He, X. Qin, S. Ramakrishna, *Chemical Engineering Journal*, 2021, **426**, 130345.

34 C. Song, K. Xia, Z. Xu, *Microelectronic Engineering*, 2022, **256**, 111723.

35 J. Yu, L. Chen, X. Hou, J. Mu, J. He, W. Geng, X. Qiao, X. Chou, *Journal of Materiomics*, 2022, **8**, 247.

36 M. Zhu, Q. Shi, T. He, Z. Yi, Y. Ma, B. Yang, T. Chen, C. Lee, *ACS Nano*, 2019, **13**, 1940.